Journal of Advanced Research 63 (2024) 195–206

Contents lists available at ScienceDirect

Journal of Advanced Research

journal homepage: www.elsevier.com/locate/jare

ASIC1/RIP1 accelerates atherosclerosis via disrupting lipophagy

Yuan-Mei Wang [a,b,1], Huang Tang [c,1], Ya-Jie Tang [d,1], Juan Liu [a], Yu-Fang Yin [e], Ya-Ling Tang [a,*], Yao-Guang Feng [f,*], Hong-Feng Gu [a,*]

[a] Department of Physiology & Institute of Neuroscience, Hengyang Medical College, University of South China, Hengyang 421001, Hunan, People's Republic of China
[b] College of Life Sciences, University of Chinese Academy of Sciences, Beijing 100049, People's Republic of China
[c] Lhasa Guangsheng Hospital, 850000 Tibet, People's Republic of China
[d] Department of Cardiovascular Surgery, Fuwai Hospital, National Center for Cardiovascular Diseases, Chinese Academy of Medical Sciences, Peking Union Medical College, Beijing, People's Republic of China
[e] Department of Neuroscience and Pharmacology, School of Medicine, Southern Illinois University Springfield, Illinois, United States
[f] Department of Cardiothoracic Surgery, The First Affiliated Hospital of University of South China, Hengyang 421001, Hunan, People's Republic of China

HIGHLIGHTS

- ASIC1 facilitates atherosclerosis via impeding lipophagy.
- ASIC1 promotes RIP1 phosphorylation.
- ASIC1-RIP1 interaction contributes to defective autophagy flux.
- ASIC1/RIP1 facilitates lipid accumulation via inhibiting lipophagy.
- ASIC1/RIP1 may be a novel target for atherosclerotic treatment.

GRAPHICAL ABSTRACT

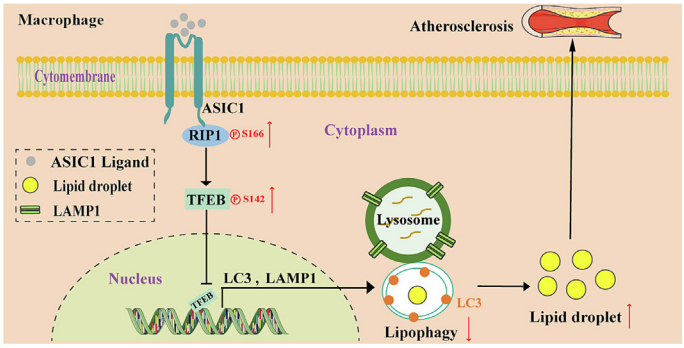

ARTICLE INFO

Article history:
Received 18 June 2023
Revised 2 November 2023
Accepted 3 November 2023
Available online 4 November 2023

Keywords:
Atherosclerosis
ASIC1
RIP1
Lipophagy
Lipid accumulation

ABSTRACT

Introduction: Atherosclerosis, a major contributor to cardiovascular disease, remains a significant health concern worldwide. While previous research has shown that acid-sensing ion channel 1 (ASIC1) impedes macrophage cholesterol efflux, its precise role in atherogenesis and the underlying mechanisms have remained elusive.

Objectives: This study aimed to investigate the role of ASIC1 in atherosclerosis and its underlying mechanisms.

Methods: First, data from a single-cell RNA sequencing (scRNA-seq) database were used to explore the relationships between ASIC1 differential expression and lipophagy in human atherosclerotic lesions. Finally, we validated the role of ASIC1/RIP1 signaling in lipophagy in vivo (human and mice) and in vitro (RAW264.7 and HTP-1 cells).

Result: Our results demonstrated a significant increase in ASIC1 protein levels within CD68+ macrophages in both human aortic lesions and AopE$^{-/-}$ mouse lesion areas compared to nonlesion regions. Concurrently, there was a notable decrease in lipophagy, a crucial process for lipid metabolism. In vitro assays further elucidated that ASIC1 interaction with RIP1 (receptor-interacting protein 1) promoted the phosphorylation of RIP1 at serine 166 and transcription factor EB (TFEB) at serine 142, leading to disrupted lipophagy and increased lipid accumulation. Intriguingly, all these events were reversed upon ASIC1 deficiency and RIP1 inhibition. Furthermore, in ApoE$^{-/-}$ mouse models of atherosclerosis, silencing

* Correspondence authors.
E-mail addresses: tangyaling7508@163.com (Y.-L. Tang), fengyaog@hotmail.com (Y.-G. Feng), ghf513@usc.edu.cn (H.-F. Gu).
[1] Yuan-Mei Wang, Huang Tang and Ya-Jie Tang contribute equal to this work.

https://doi.org/10.1016/j.jare.2023.11.004

ASIC1 expression or inhibiting RIP1 activation not only significantly attenuated atherogenesis but also restored TFEB-mediated lipophagy in aortic tissues. This was evidenced by reduced TFEB Ser-142 phosphorylation, decreased LC3II and LAMP1 protein expression, increased numbers of lipophagosomes, and a decrease in lipid droplets.

Conclusion: Our findings unveil the critical role of macrophage ASIC1 in interacting with RIP1 to inhibit lipophagy, thereby promoting atherogenesis. Targeting ASIC1 represents a promising therapeutic avenue for the treatment of atherosclerosis.

Introduction

Atherosclerosis, a disease caused by the accumulation of cholesterol-rich plaques in large arteries, results in myocardial infarction and stroke and is the major cause of morbidity and mortality worldwide. In addition to traditional factors for atherosclerosis, acidification of the intimal fluid may play a crucial role in the pathogenesis of this disease. Acidification, a likely consequence of intimal activated macrophages, generates and extrudes glycolytic products, such as lactic acid and protons, into the intimal fluid, leading to acidification of the extracellular environment [1]. Growing studies have revealed that this acidic extracellular pH promotes lipid uptake and compromises cholesterol efflux from macrophage foam cells, thereby facilitating atherosclerosis development [2]. Recently, Liu et al. reported that preventing the acidification of intimal fluid profoundly decreases atherosclerotic lesions in ApoE$^{-/-}$ mice [3]. Although studies have solidly confirmed that extracellular acidity is a critical contributor to atherogenesis and plaque vulnerability, the underlying mechanisms have not been fully illustrated. Therefore, it is imperative to clarify these mechanisms to uncover potential therapeutic targets for atherosclerosis.

Acid-sensing ion channels (ASICs), a group of proton-gated cation channels, are widely expressed in various tissues and activated by extracellular low pH [4,5]. To date, seven ASIC members, ASIC1a, ASIC1b, ASIC1b2, ASIC2a, ASIC2b, ASIC3, and ASIC4, have been identified. Among them, ASIC1 is the most sensitive to extracellular protons and can even be activated by pH values lower than 7.0 [6]. ASIC1a, ASIC1b and ASIC1b2 are splice isoforms of ASIC1, which differ in the N-terminal third of their protein sequences and exhibit distinct channel properties. It has been demonstrated that ASIC1 plays a critical role in a series of pathological processes associated with tissue acidity, such as neuronal disorder diseases, ischemic stroke, and osteoarthritis [7,8]. Interestingly, our recent studies show that blockade of ASIC1 by psalmotoxin 1 (a specific inhibitor of ASIC1) obviously prevents extracellular acidity-induced macrophage foam formation and promotes ATP binding cassette transporter A1 (ABCA1)-dependent cholesterol efflux [9]. Given that foam cell formation is a primary event in atherogenesis, ASIC1 may play a critical role in the pathogenesis of atherosclerosis. However, the mechanisms by which this channel contributes to atherosclerosis remain unclear.

Lipophagy is a selective autophagy that delivers intracellular cholesteryl ester-rich lipid droplets (LDs) to lysosomes for degradation into free cholesterol, which can then be effluxed through ABCA1 [10]. Consequently, lipophagy deficiency can impede LD degradation and cholesterol efflux, resulting in excess lipid accumulation. Indeed, defective lipophagy has been identified in lipid overaccumulation diseases such as fatty liver and atherosclerosis [11]. It has been reported that transcription factor EB (TFEB) is the master regulator of lipophagy by promoting the expression of autophagy and lysosomere-related genes (such as LC3 and LAMP1) [12]. The phosphorylation sites of TFEB govern its transcriptional activity by controlling the nuclear translocation of this transcription factor [13]. Recent studies have indicated that receptor-interacting protein 1 (RIP1), a serine-threonine kinase, negatively regulates autophagy by promoting the phosphorylation of TFEB at Ser142 [14]. Notably, Wang YZ et al. demonstrated that the activation of ASIC1 promotes RIP1 phosphorylation by recruiting RIP1 to the ASIC1 C-terminus in neurons in response to tissue acidity [15]. Furthermore, studies have shown that ASIC1 plays a critical role in acidity-induced activation of autophagy in rat articular chondrocytes [16]. However, it remains unclear whether the RIP1-TFEB pathway is involved in ASIC1-mediated lipophagy in atherosclerosis.

In the present study, we first identified the association of macrophage ASIC1 expression and lipophagy deficits in both human and murine atherosclerotic lesions using scRNA-seq database analyses and immunofluorescence staining. We then clarified whether ox-LDL-induced macrophage foam cell formation was the result of ASIC1-RIP1 activation to inhibit lipophagy in RAW264.7 cells. Furthermore, we explored the influences of ASIC1 silencing or RIP1 inhibition on aortic lipophagy and atherosclerosis in ApoE$^{-/-}$ mice. We found that ASIC1 was abundantly expressed, while lipophagy was dramatically impeded in atherosclerotic plaques. In vitro results indicated that ox-LDL exposure promoted the ASIC1-RIP1 interaction followed by decreased lipophagy, thereby facilitating lipid accumulation. In vivo findings further confirmed that blockade of the ASIC1-RIP1 pathway markedly restored macrophage lipophagy, leading to a decrease in atherosclerotic lesions. Taken together, this study reveals the role of ASIC1 and its underlying mechanism in atherosclerosis, providing ASIC1 as a potential new therapeutic target for this disease.

Methods and materials

Materials

Ox-LDL was purchased from Yiyuan Biotechnology (Guangzhou, China); Oil Red O (ORO) was obtained from Sigma–Aldrich (United States); Chloroquine diphosphate (CQ) and Necrostatin-1 (Nec-1) were from Selleck (United States); DAPI was bought from Solarbio (Beijing, China); BODIPY was from Thermo Scientific (United States); Phospho-TFEB (Ser142) antibody was bought from Affinity Biosciences (China); Anti-CD68 antibodies were from Abcam (United Kingdom); Anti-RIP1, -p-RIP1, -p62, and -LC3 antibodies were purchased from Cell Signaling Technology (United States); Anti-β actin and -ASIC1 antibodies were provided by Proteintech (United States); Anti-LAMP1 antibody was obtained from Beyotime Biotechnology (Shanghai, China); Alexa Fluor® 488 goat anti-rabbit antibodies and Alexa Fluor® 594 goat anti-mouse antibodies were from Jackson TmmunoResearch (United States). HBLV-m-Asic1 shRNA-ZsGreen-PURO (LV-ASIC1 siRNA) and HBLV-ZsGreen-PURO NC (LV-Control) were obtained from Hanbio Biotechnology Co. Ltd. (Shanghai, China).

scRNA-seq data retrieval and preprocessing

The single-cell RNA sequencing (scRNA-seq) data used in this study were obtained from the Gene Expression Omnibus (GEO)

under the accession numbers #GSE159677, which comprised six samples, and #GSE201333, which included one sample. The #GSE159677 dataset consisted of three pairs of atherosclerotic lesions and corresponding proximal adjacent carotid arteries from patients. The #GSE201333 dataset included one sample from a normal coronary artery. For data analysis, we processed the scRNA-seq data in the R programming environment utilizing the 'Seurat 4.3.0′ package [17]. To ensure data quality, we removed cells that exhibited more than 10% mitochondrial gene expression. We conducted a principal component analysis (PCA) using genes identified as highly variable by the "FindVariableGenes" function. Subsequently, we selected the most appropriate principal components (PCs) for clustering, employing specific resolution parameters. To mitigate batch effects, we applied the 'harmony 0.1.0′ algorithm. After classifying cell types, we conducted Gene Ontology (GO) analysis to identify cell type-specific pathways between normal and atherosclerotic tissues. This analysis was performed using the 'clusterProfiler 4.7.1.2′ package [18].

Ethics statement

All experiments involving human samples were carried out in accordance with the guidelines and regulations set forth by the Ethics Committee of the First Affiliated Hospital of the University of South China (Ethics Committee Protocol Number: 2021015). Informed consent was obtained from all patients who participated in the study after providing them with detailed information regarding the study's objectives.

In compliance with both institutional and national guidelines for the ethical treatment of animals, all procedures involving animals were conducted in this study. The study's animal protocols were subject to approval by the Animal Experimentation Ethics Committee of the University of South China (Permit Number: 20210308). All animal-related activities were performed in strict adherence to ethical standards and guidelines governing the care and use of animals.

Human samples and treatment

Human aortic plaques were obtained from a total of eight patients. Among these samples, five were subjected to fixation with 4% paraformaldehyde for 24 h. These fixed samples were subsequently sectioned into consecutive slices for various analyses, including Oil Red O (ORO) staining, hematoxylin and eosin (H&E) staining, and immunofluorescence staining. The remaining three samples were preserved at a temperature of −80 °C for subsequent protein expression analysis. This approach allowed for a comprehensive examination of the aortic plaques obtained from the patient cohort.

Hematoxylin and eosin (H&E) staining

The sections obtained from atherosclerotic segments and nonlesion regions underwent the following staining procedure: Sections were initially immersed in hematoxylin for several minutes and then rinsed with tap water. Afterward, a brief differentiation step was carried out using 1% hydrochloric acid alcohol, followed by another rinse with tap water. Subsequently, they were counterstained with a 1% ammonia water solution for 1 min and rinsed briefly under running water. Finally, the sections were stained with eosin for a few seconds and rinsed again under running water. These steps aimed to assess changes in cell morphology within the blood vessels, and the evaluation was conducted using a microscope.

Mice and treatment

Fifty male ApoE$^{-/-}$ mice, with a C57BL/6J background, weighing between 18.0 and 19.0 g and aged 6 weeks, were procured from the Model Animal Research Center of Nanjing University, China. These mice were maintained under standard housing conditions, with a temperature of 23 ± 1 °C and a 12-hour light/12-hour dark cycle. They had unrestricted access to both water and a standard diet. Following a one-week period of acclimation, the mice were subjected to various treatments. Some received LV-Control or LV-ASIC1 siRNA (1×10^7 TU/mouse) via a single tail vein injection, while others were administered the RIP1-specific inhibitor Nec-1 (2 mg/kg per day) through intraperitoneal injection. All mice were then placed on a high-fat diet for a duration of 12 weeks before being euthanized for further analysis. All animal-related procedures were conducted in accordance with the ethical standards and guidelines established by the Animal Experimentation Ethics Committee of the University of South China under Permit Number: 2018012.

Atherosclerotic lesion analysis

After the 12-week treatment, the mice were humanely euthanized using carbon dioxide narcosis. The hearts and aortas were carefully extracted from the mice following perfusion with PBS through the left ventricle. The entire aorta, spanning from the proximal ascending aorta to the abdominal aortic bifurcation, was immersed in a 4% paraformaldehyde solution. The adventitial fat was removed, and then the aortas were longitudinally cut open. This was done in preparation for Oil Red O (ORO) staining to quantify atherosclerotic lesion surface areas when examining the aortas en face. Additionally, the base of the heart, which is connected to the aortic root, was preserved in OCT compound after overnight fixation in 4% paraformaldehyde. Subsequently, serial cryostat sections with a thickness of 8 μm were generated for ORO staining to assess atherosclerotic lesions in the aortic sinus. Images of the stained sections were captured using a light microscope, and the quantification of these lesions was performed with Image-Pro Plus 6.0 software. The data are presented as the average lesion size per section or as a percentage of the total aortic surface area. For each mouse, an average of 10 sections was analyzed during this process.

Immunofluorescence staining

Aortic root frozen sections or cultured RAW 264.7 cells were fixed in 4% paraformaldehyde solution for 15 min, followed by permeabilization with 0.1% Triton X-100 in PBS. After incubation in 2% BSA for 1 h, the samples were incubated with primary antibodies against CD 68 (1:100), ASIC1 (1:100), LAMP1 (1:100), and LC3 (1:100) at 4 °C overnight. After washing three times (10 min) with PBS, the slices were incubated with fluorescently labeled secondary antibodies or BODIPY for neutral lipid staining for 1 h at room temperature. Subsequently, the nuclei were labeled by DAPI. Finally, the stained samples were imaged by fluorescence microscopy (Thermo Scientific, China) or confocal laser scanning microscopy (Zeiss LSM980 Airyscan 2, Germany).

Cell culture and treatment

RAW 264.7 macrophages were provided by the Institute of Cardiovascular Disease, University of South China. Cells were incubated in RPMI 1640 medium (Invitrogen, United States) containing 10% fetal bovine serum (FBS, Thermo, United States). To assess lipid accumulation in macrophages, the cells were incubated with 25 μg/mL ox-LDL for 24 h. For pharmacological intervention, the cells were cocultured with the RIP1 inhibitor Nec-1 and the autop-

hagy–lysosome inhibitor CQ for 24 h. For genetic knockdown, macrophages were transfected with LV-ASIC1 or siRNA LV-Control siRNA for 48 h according to the manufacturer's instructions. Immunoblotting was used to confirm the transfection efficiency of LV-siRNA.

The THP-1 cell line was obtained from the Institute of Cardiovascular Disease, University of South China. Cells were cultured in RPMI 1640 medium containing 10% FBS. When the cell density reached 90% or higher, the cells were induced into macrophage-like phenotype cells by treatment with 100 ng/mL phorbol-12-myristate-13-acetate (PMA) for 24 h. Then, macrophages were treated with ox-LDL (50 μg/mL, except for the control group), PcTx-1 (10 ng/mL), or Nec-1 (20 μM) for 24 h.

ORO staining

Cultured RAW 264.7 macrophages were plated on cover slides in six-well plates (2×10^5 cells/well) and incubated with the indicated reagents for 24 h. The macrophages were fixed with 4% paraformaldehyde for 30 min, followed by washing 3 times with PBS. The fixed macrophages were stained with ORO for 30 min at 37 ℃ and then counterstained with hematoxylin. Lipid accumulation was viewed under a light microscope (Thermo Scientific, China), and images were photographed. The ORO-positive areas were quantified by ImageJ software.

Western blot analysis

Cultured macrophages or harvested aortas were extracted with RIPA buffer containing complete protease and phosphatase inhibitors on ice. Cytosolic and nuclear proteins were prepared with a nuclear/cytosol fractionation kit (Beyotime, Beijing, China). The total protein concentration was measured by a BCA kit (Beyotime, China). Then, equal amounts of boiled protein samples (10 μl) were separated by sodium dodecyl sulfate–polyacrylamide gel electrophoresis (SDS–PAGE), followed by transfer onto PVDF membranes (Millipore, United States). Subsequently, the membranes were incubated with primary antibodies against ASIC1 (1: 500), RIP1 (1: 1000), p-RIP1 (1: 500), p62 (1: 1000), LAMP1 (1: 500), LC3 (1: 1000), p-TFEB -Ser 142 (1: 500); β-actin (1: 1000) at 4 ℃ overnight, respectively. Subsequently, the membranes were incubated with HRP-conjugated secondary antibodies. Finally, immunoreactive bands were visualized by an enhanced chemiluminescence (ECL) detection system, and the band intensity was analyzed with Image Lab software.

Cholesterol efflux

RAW 264.7 macrophages were plated at a density of 1×10^5 cells/well in a 96-well tissue culture plate using 100 μl growth medium (RPMI 1640 with 10% FBS) per well for 6 h. Then, 100 μl of the labeling medium mix was added to each well. The plate was incubated for 1 h. Subsequently, the cells were incubated in medium containing 25 μg/mL ox-LDL (except the control group) with or without PcTx1 (10 ng/mL) or Nec-1 (20 μM) for an additional 24 h. Intracellular cholesterol content was measured using the ab196985 – Cholesterol Efflux Assay Kit (Abcam) according to the manufacturer's instructions.

Transmission electron microscopy

After being dissected from the mice, aortic roots were quickly cut into small blocks (1 mm^3) and fixed in 2.5% glutaraldehyde overnight at 4 ℃. The tissues were then postfixed with 1% osmium tetroxide and dehydrated in an ascending series of ethanol. Subsequently, the samples were embedded in poly/Bed-812 resin, followed by being cut into ultrathin sections. Finally, the sections were stained with uranyl acetate and lead citrate. Images were photographed by a transmission electron microscope (TEM, JEM-1200EX; JEOL, Tokyo, Japan). For quantification of lipophagy, lipophagosomes (LPs, defined as autophagosomes, double-membraned structures containing lipid droplets) were counted.

Statistical analysis

The data are expressed as the mean ± SEM based on at least three independent experiments. Statistical analysis was performed by using GraphPad Prism 9 software. Student's *t* test was used for two-group or one-way ANOVA with Bonferroni post hoc correction used for multiple-group comparisons. Statistical significance was defined as $P < 0.05$.

Results

Sing-cell landscape of macrophage clusters in human atherosclerotic plaques

To delve into the cell clusters involved in atherosclerosis pathogenesis, our initial step involved elucidating the gene expression profiles within the human atherosclerotic core (AC), patient-matched proximal adjacent carotid arteries (PC), and normal coronary artery (NC). We achieved this by utilizing the scRNA-seq database obtained from GEO (accession # GSE159677 and # GSE201333). Following a meticulous cell filtering process, we successfully identified and categorized a total of 48,952 individual cells into 10 distinct clusters based on marker genes [19], as depicted in Fig. 1A. To ensure the accuracy of our cell cluster classification, we annotated the 10 primary cell types based on their marker gene expression, as illustrated in Fig. 1B. Among these cell clusters, the cell type expressing CD 14 and CD 68 markers was predominantly identified as macrophages. This classification was further validated through a volcano plot displaying the top 5 ranking genes (Fig. 1C). Furthermore, we assessed the distribution of cell types within each sample. The results clearly indicated a significant abundance of macrophages within the human AC compared to PC and NC (Fig. 1D). These findings align with previous research [20].

ASIC1 is abundantly expressed in macrophages within atherosclerotic lesions

Building upon our previous study, which showed the expression of ASIC1 in RAW 264.7 macrophages, we proceeded to evaluate the expression of ASIC1 mRNA in both normal coronary arteries (NC) and atherosclerotic cores (AC) through the analysis of differentially expressed genes. As depicted in the volcano plots (Fig. 2A and B), our findings reveal that there is no statistically significant difference in ASIC1 mRNA expression within the context of both 10 cell clusters (Fig. 2A) and specifically within macrophages (Fig. 2B). To gain deeper insights into the protein expression of ASIC1 in atherosclerosis (AS), we performed Western blotting assays on segments obtained from patients, including self-nonlesion and atherosclerotic segments. The outcomes of our analysis unmistakably revealed a substantial upregulation of ASIC1 expression in atherosclerotic segments when compared to the control (Fig. 2C). Furthermore, our findings were corroborated by both Oil Red O (ORO) staining and hematoxylin and eosin (H&E) staining results, which clearly indicated a significant increase in lipid deposition (depicted as the red area) within atherosclerotic segments as opposed to self-nonlesion segments (Fig. 2D).

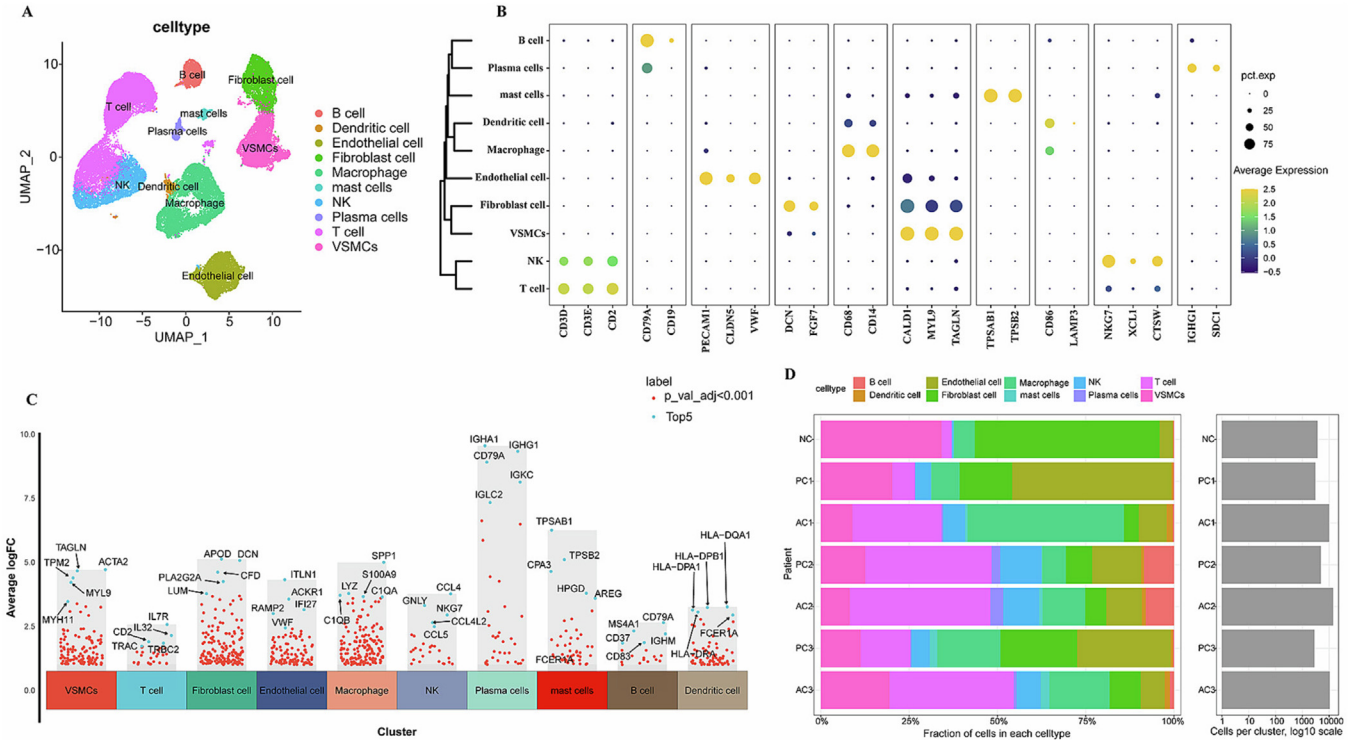

Fig. 1. *The single-cell transcriptional landscape of human atherosclerotic lesions.* (A) The UMAP map illustrates the distribution of the 10 cell clusters. NK: natural killer cells, VSMCs: vascular smooth muscle cells. (B) DotPlot provides an indication of marker gene expression within each cell cluster. (C) The volcano plot shows the top 5 ranking genes in each cell cluster. (D) The chart displays the percentage of each cell cluster in each sample. AC: atherosclerotic core, PC: patient-matched proximal adjacent tissue, NC: normal control tissue.

Interestingly, our investigation unveiled a predominant expression of ASIC1 within macrophages localized specifically within atherosclerotic lesions. This was clearly substantiated by the colocalization (highlighted by white arrows) of ASIC1 (in green) with CD68-positive regions (in red), as depicted in Fig. 2E. These findings were consistently observed in atherosclerotic lesions in ApoE$^{-/-}$ mice (Fig. 2F). Collectively, these results strongly imply that ASIC1 is abundantly expressed within atherosclerotic plaques and demonstrates close colocalization with macrophages. This suggests that macrophage ASIC1 may indeed play a pivotal role in the causal relationship with atherogenesis.

Lipophagy is impaired in both human and mouse atherosclerotic lesions

In light of ASIC1 upregulation in atherosclerotic lesions and its potential role in autophagy dysregulation [21], we embarked on an exploration of alterations in autophagy-associated pathways within atherosclerotic cores (AC) and normal coronary arteries (NC). Our investigation utilized a multifaceted approach encompassing scRNA-seq analysis, immunofluorescence staining, and transmission electron microscopy assays. The outcomes of our GO analysis revealed a profound decrease in macroautophagy within macrophages residing in atherosclerotic lesions, as illustrated in Fig. 2G. Furthermore, the volcano plots underscored a significant reduction in LAMP1 expression within macrophages in human AC when compared to that in the NC (Fig. 2H). These findings collectively point toward a deficiency in autophagy occurring in macrophages within atherosclerotic lesions.

To further validate whether lipophagy was impaired in the context of atherosclerosis, we conducted an assessment of double-membrane autophagy vesicles and lipid droplets (LDs) in both human self-nonlesion regions and atherosclerotic segments, as depicted in Fig. 2I and J. Our immunofluorescence staining results unequivocally revealed a significant reduction in the colocalization areas of LC3II (a hallmark of autophagy) with BODIPY (a marker for LDs) and LAMP1 with BODIPY within human atherosclerotic lesions in comparison to self-nonlesion regions. These findings compellingly indicate the presence of lipophagy deficiency. Furthermore, our transmission electron microscopy (TEM) results also demonstrated a marked inhibition of lipophagy in ApoE$^{-/-}$ mouse plaques when contrasted with normal control aortic roots. This was evident through the increased number of LDs and a concurrent decrease in the number of lipid-protein complexes (LPs) (Fig. 2K). Collectively, these results serve as strong evidence that defective lipophagy is indeed prevalent in both human and mouse atherosclerotic lesions.

ASIC1 promotes RIP1 phosphorylation in both RAW 264.7 and THP-1 macrophages

Prior research has established that extracellular acidity induces an ASIC1-RIP1 interaction, leading to RIP1 phosphorylation in neurons and consequent ischemic neuronal injury [15]. Therefore, we investigated whether such an interaction occurs in RAW 264.7 and THP-1 macrophages induced by ox-LDL. To test this hypothesis, macrophages were cultured with or without 25 μg/ml ox-LDL, and we validated the ASIC1-RIP1 association by a coimmunoprecipitation (Co-IP) assay (Fig. 3A). Our results indicated that ASIC1 did indeed interact with RIP1 in RAW264.7 macrophages, and ox-LDL seemed to enhance their association. Moreover, the level of RIP1 phosphorylation at Ser-166 (p-RIP1Ser-166) was also significantly increased (Fig. 3A), which was abolished by the ASIC1-specific inhibitor PcTx1. To clarify the possibility that ASIC1 was upstream of RIP1, RAW264.7 macrophages were treated with LV-control, LV-ASIC1 siRNA, and the RIP1 inhibitor Nec-1 in the pres-

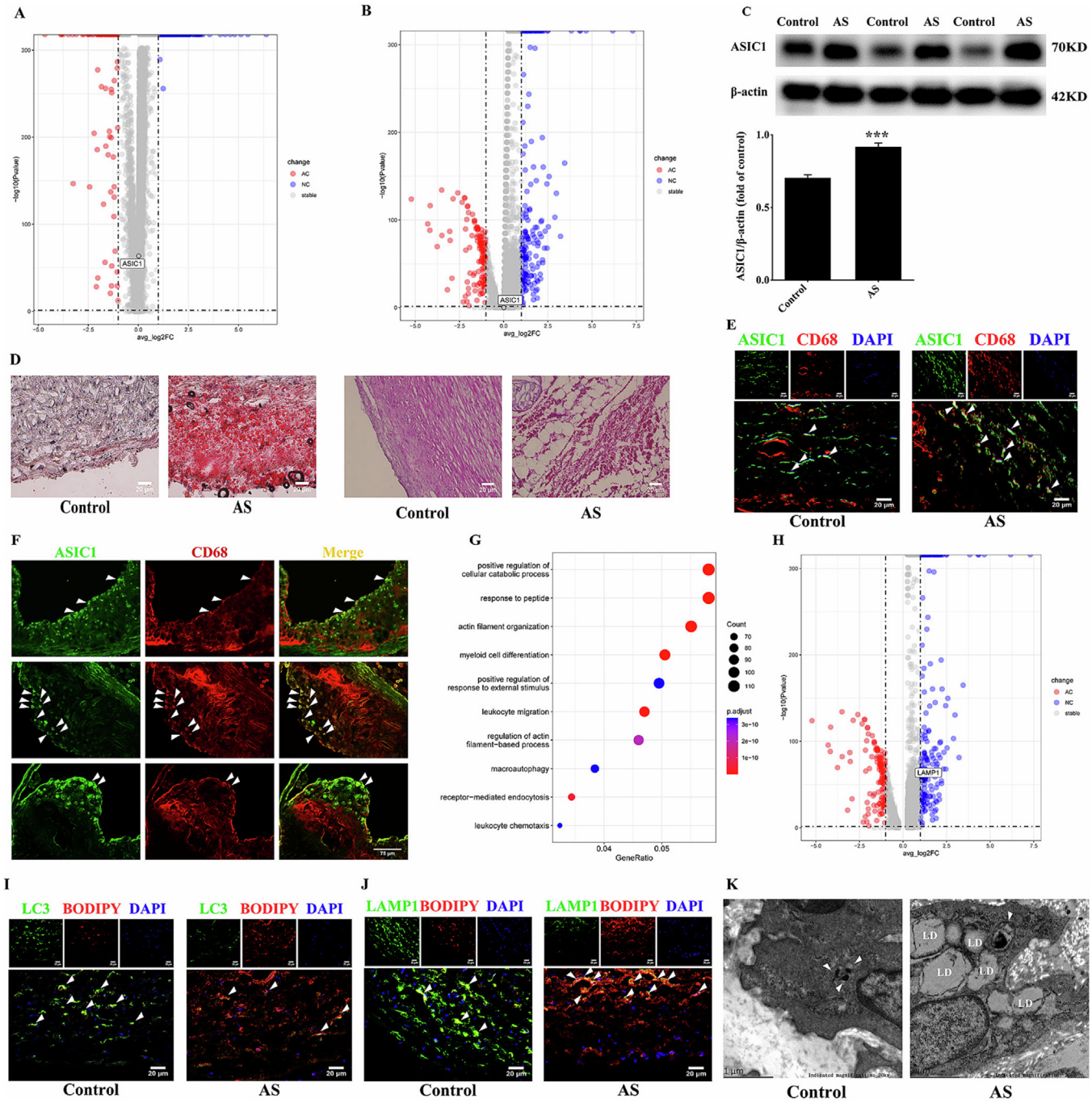

Fig. 2. *Changes in ASIC1 and lipophagy in atherosclerotic lesions.* (A, B) The volcano plot displays differentially expressed genes in the whole cell type (A) and within the macrophage cluster (B), comparing self-nonlesion regions to atherosclerotic segments. AC: human atherosclerotic core, NC: normal coronary artery. (C) Depicting the ASIC1 protein level in self-nonlesion and atherosclerotic segments from patients with atherosclerosis (AS). (D) Representative images of Oil Red O (ORO) and hematoxylin and eosin (H&E) staining of the human thoracic aorta. (E) Immunofluorescence analysis of ASIC1 (in green) expression in CD68 macrophages (in red) within the human aorta. DAPI (in blue) stains the nuclei. The white arrows indicate coexpressed regions. Scale bar: 20 μm. (F) Immunofluorescence analysis of the colocalization of ASIC1 (in green) with CD68 (in red) in the aortic root from ApoE$^{-/-}$ mice. Three different sections of the aortic root are presented. The white arrows indicate coexpressed regions. Scale bar: 75 μm. (G) Bubble plots illustrate GO-enriched items of differentially expressed genes in the human atherosclerotic core. (H) The volcano plot illustrates differentially expressed genes in the macrophage cluster within self-nonlesion regions and atherosclerotic segments. (I, J) Immunofluorescence analysis of the colocalization of BODIPY with LC3 (I) and BODIPY with LAMP1 (J) within the human aorta. The white arrows represent coexpressed regions. Cell nuclei are stained with DAPI. Scale bar: 20 μm. (K) Analysis of the morphology of lipophagy in the aortic roots of ApoE$^{-/-}$ mice using transmission electron microscopy. The white arrows represent lipophagosomes. LD: lipid droplets, Scale bar, 1 μm. (For interpretation of the references to colour in this figure legend, the reader is referred to the web version of this article.)

ence or absence of 25 μg/ml ox-LDL. Western blotting assays were performed to measure the expression of ASIC1, RIP1, and p-RIP1 (Fig. 3B and C). The results demonstrated that LV-ASIC1 siRNA significantly lowered ASIC1 expression and the p-RIP1/RIP1 ratio in macrophages challenged with ox-LDL. Nec-1 treatment only profoundly decreased the proportion of p-RIP1/RIP1 (Fig. 3B) but had no significant influence on the expression of ASIC1 (Fig. 3C). Similar results were demonstrated in THP-1 macrophages treated with PcTx1 or Nec-1 (Supplementary Fig. 1). Collectively, these results imply that ASIC1 is upstream of RIP1 and that ox-LDL

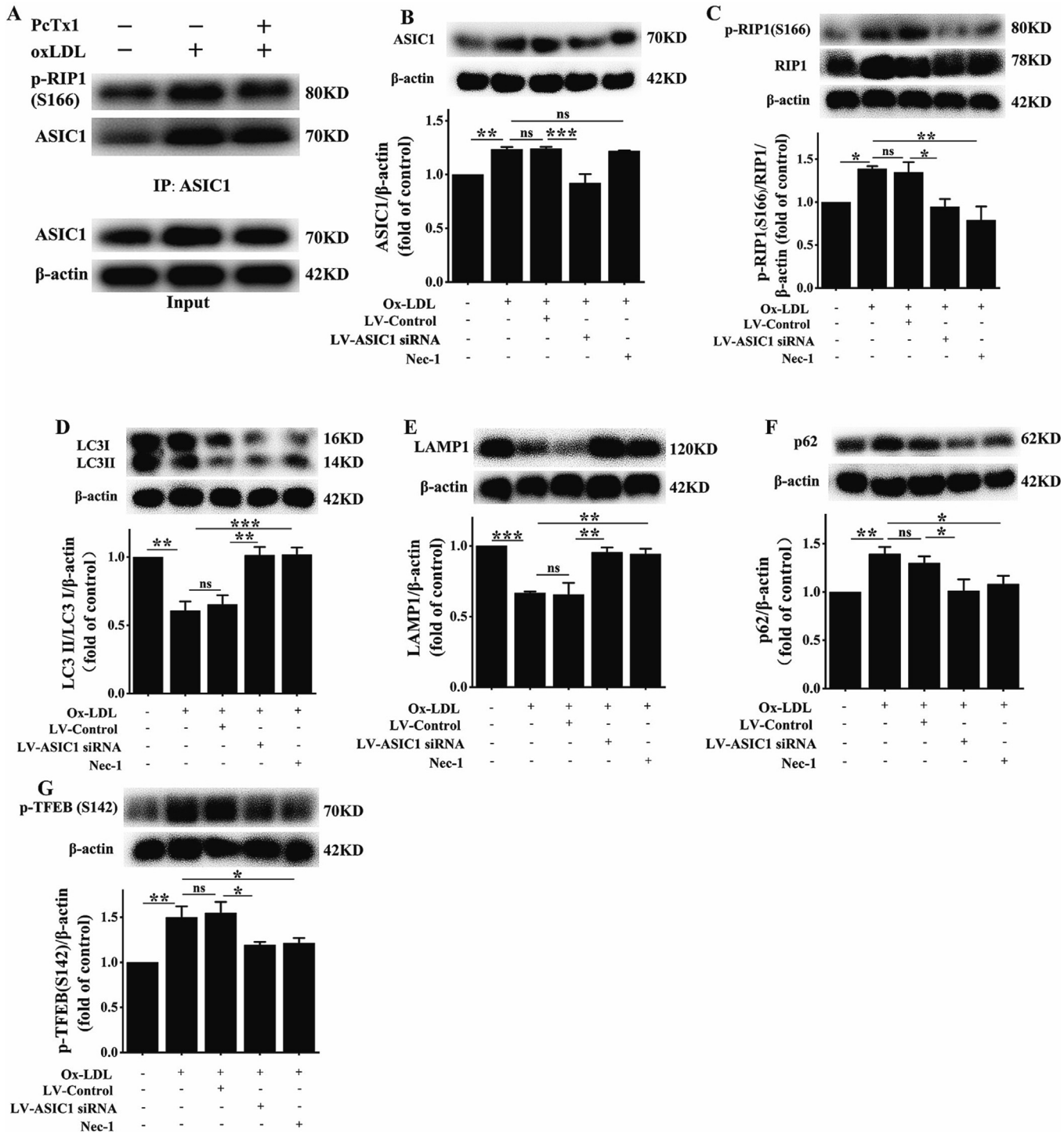

Fig. 3. *Effect of ASIC1/RIP1 on autophagy in RAW 264.7 macrophages.* RAW 264.7 macrophages were cultured with 25 μg/mL ox-LDL in the presence or absence of PcTx1 (100 ng/ml) for 24 h. (A) Co-IP was used to evaluate the interaction between ASIC1 and RIP1. (B-G) RAW 264.7 macrophages were cultured with 25 μg/mL ox-LDL with or without LV-Control, LV-ASIC1 siRNA and RIP1 inhibitor (Nec-1). Western blotting analyses were performed to determine ASIC1 expression and RIP1 phosphorylation, as well as LC3I and LC3II, p62, and LAMP1 expression and TFEB phosphorylation. All data are presented as the mean ± SEM. $^{*}P < 0.05$, $^{**}P < 0.01$, $^{***}P < 0.001$.

treatment facilitates the ASIC1-RIP1 interaction and subsequent RIP1 phosphorylation.

ASIC1-RIP1 association contributes to defective autophagy flux in both RAW 264.7 and THP-1 macrophages induced by ox-LDL

It has been confirmed that phosphorylation of TFEB at serine 142 induced by p-RIP1ser 166 prevents nuclear translocation of TFEB and subsequently decreases the transcription of autophagy and lysosomal genes [22]. Moreover, our above results indicate that ox-LDL promotes the association of ASIC1 and RIP1 and RIP1 phosphorylation. Hence, we investigated how and by which the ASIC1/RIP1 pathway influenced autophagic flux in RAW 264.7 macrophages. To clarify the effect of the ASIC1/RIP1 pathway on autophagic flux in RAW 264.7 macrophages, three specific markers of autophagic flux, the LC3II/LC3I ratio and LAMP1 and p62 protein

levels, were analyzed by Western blotting. As shown in Fig. 3D–F, autophagic flux was impaired in ox-LDL-induced macrophages, as indicated by a significant decrease in the ratio of LC3II/LC3I and level of LAMP1 and an increase in the protein level of p62. However, treatment with LV-ASIC1 siRNA or the RIP1-specific inhibitor Nec-1 dramatically reversed the ox-LDL-induced defective autophagic flux in macrophages, demonstrating that the ASIC1/RIP1 association results in autophagic flux impairment.

We then further investigated whether TFEB was involved in ASIC1/RIP1-mediated autophagic flux deficiency in macrophages. TFEB is responsible for the transcription of a large number of autophagic flux-related genes, including LC3, p62 and LAPM1 [23,24]. Moreover, previous studies have indicated that TFEB phosphorylation at serine 142 inhibits autophagy by preventing its nuclear translocation [13]. Our Western blotting results indicated that p-TFEB Ser-142 was significantly elevated in RAW 264.7 macrophages treated with ox-LDL compared with control macrophages. Of note, such an increase in p-TFEB Ser-142 was obviously abolished by treatment with LV-ASIC1 siRNA or RIP1-specific inhibitor Nec-1 (Fig. 3G), suggesting that ASIC1-RIP1 association facilitates phosphorylation of TFEB at serine 142. Similar results were observed in THP-1 cells (Supplementary Fig. 1). Taken together, these results show that the ASIC1-RIP1 association causes autophagic flux impairment in RAW 264.7 macrophages treated with ox-LDL, and the underlying mechanism may involve TFEB phosphorylation.

ASIC1/RIP1 facilitates lipid accumulation in RAW 264.7 macrophages by inhibiting lipophagy

To verify whether the association between ASIC1 and RIP1 leads to the disruption of lipophagy and subsequent lipid accumulation, we treated ox-LDL-induced RAW 264.7 macrophages with LV-ASIC1 siRNA, the RIP1 inhibitor Nec-1, and the autophagy–lysosome inhibitor CQ. Lipophagy was analyzed by visualizing the colocalization of BODIPY with LC3 or LAMP1 using laser confocal microscopy. As shown in Fig. 4A and B, a large amount of LDs were observed in the ox-LDL group, but few of them colocalized with LC3 (Fig. 4A) or LAMP1 (Fig. 4B), indicating that both the formation of LDs and their fusion with lysosomes for degradation might be inhibited. As expected, pretreatment with LV-ASIC1 siRNA or Nec-1 effectively restored macrophage lipophagy, as evidenced by a significant increase in the colocalization of LDs with LC3 and LAMP1. This beneficial effect of LV-ASIC1 siRNA and Nec-1 on lipophagy was cancelled by CQ. These results reveal that the association between ASIC1 and RIP1 results in the disruption of lipophagy in macrophages.

Considering that lipophagy promotes LD degradation into free cholesterol for efflux, thus preventing overloaded lipid accumulation, the effect of ASIC1-RIP1-mediated lipophagy deficiency on macrophage foam cell formation was investigated using ORO staining and cholesterol efflux assays (Supplementary Fig. 2). As shown in Fig. 4C and 4D, in line with the disruption of lipophagy, lipid aggregation in macrophages treated with ox-LDL notably increased compared to that in control macrophages. Additionally, autophagosome degradation increased lipid deposition. Pretreatment with both LV-ASIC1 siRNA and Nec-1 significantly ameliorated lipid accumulation in macrophages in the presence of ox-LDL, which was abolished by CQ. Furthermore, cholesterol efflux assay results demonstrated that the percentage of cholesterol efflux was profoundly decreased in ox-LDL-treated RAW264.7 macrophages, which can be rescued by PcTx1 and nec-1 treatment. Collectively, these results indicate that the ASIC1-RIP1 interaction disrupts lipophagy, thereby promoting lipid accumulation in macrophages.

ASIC1/RIP1 inhibition attenuates atherosclerosis in ApoE$^{-/-}$ mice

The above in vitro results established that ASIC1-RIP1 activation exacerbates macrophage lipid accumulation by compromising lipophagy. We then investigated its proatherosclerotic role in ApoE$^{-/-}$ mice by inhibiting the ASIC1/RIP1 pathway. As shown in Fig. 5A and 5B, compared to the LV-control group, the expression of ASIC1 protein in the aortas of the LV-ASIC1 siRNA group was significantly decreased. Moreover, the p-RIP1 level was profoundly lower in both the LV-ASIC1 siRNA and Nec-1 groups than in the control group, indicating that ASIC1 siRNA or Nec-1 treatment effectively prevented RIP1 activation. Interestingly, along with the inactivation of the ASIC1/RIP1 signaling pathway, atherosclerotic lesions in the aortic sinus were significantly ameliorated in both the LV-ASIC1 siRNA and Nec-1 groups compared to the control group (Fig. 5C, D). Similar changes in atherosclerotic lesions were observed in the entire aorta (Fig. 5E, F). Together, these results demonstrate that the activation of the ASIC1/RIP1 pathway promotes atherosclerosis in ApoE$^{-/-}$ mice.

Inactivation of ASIC1/RIP1 rescues lipophagy in ApoE$^{-/-}$ mice

Since ASIC1/RIP1 inactivation prevents TFEB phosphorylation and eventually restores macrophage lipophagy in vitro, we investigated whether a similar mechanism occurs in the aortas of ApoE$^{-/-}$ mice. We first measured the level of p-TFEB Ser142, a direct downstream target of p-RIP1. In line with the in vitro results, Western blot analysis demonstrated that the p-TFEB level was markedly decreased in the aortas of both the LV-ASIC1 siRNA and RIP1 groups compared to the control group (Fig. 5G). This was accompanied by a markedly increased level of LAMP1 and a markedly increased ratio of LC3II/LC3I and a reduction in p62 protein expression in the aortas, revealing that inhibition of ASIC1/RIP1 rescued autophagic flux in the aortas of ApoE$^{-/-}$ mice (Fig. 5H–J). Moreover, we characterized the influence of ASIC1/RIP1 inactivation on lipophagy in the aortic root of ApoE$^{-/-}$ mice by TEM observation. As shown in Fig. 5K, a large number of LDs accumulated in the control group mice, while LPs, the lipophagic structure, were absent within the aorta cells. However, both the LV-ASIC1 siRNA and Nec-1 treatment not only significantly decreased the number of LDs but also increased the amounts of LPs within the aorta cells. Taken together, these results imply that inactivation of ASIC1/RIP1 restores TFEB-mediated lipophagy and thereby promotes LD degradation within aortic cells, eventually impeding atherogenesis.

Discussion

This study represents the first confirmation of high ASIC1 expression in intraplaque CD68 + cells in both patients and atherosclerotic mice. Intriguingly, we observed a significant impairment in lipophagy within plaque macrophages. Furthermore, our experiments with ox-LDL exposure demonstrated the activation of the ASIC1/RIP1 pathway, leading to lipophagy deficiency and lipid accumulation in RAW 264.7 macrophages. These effects were dramatically reversed by silencing ASIC1 or inhibiting RIP1. Additionally, when we blocked the ASIC1/RIP1 pathway, we observed a rescue of lipophagy within aortic cells and an amelioration of atherosclerotic lesions in ApoE$^{-/-}$ mice. Our study further delved into the underlying mechanism, revealing that ASIC1 interacts with RIP1 to phosphorylate TFEB at serine 142. This phosphorylation event resulted in a decrease in autophagosome formation and lysosome biogenesis, thereby disrupting macrophage lipophagy. Collectively, our findings not only unveil a novel mechanism through which the ASIC1/RIP1 pathway contributes to

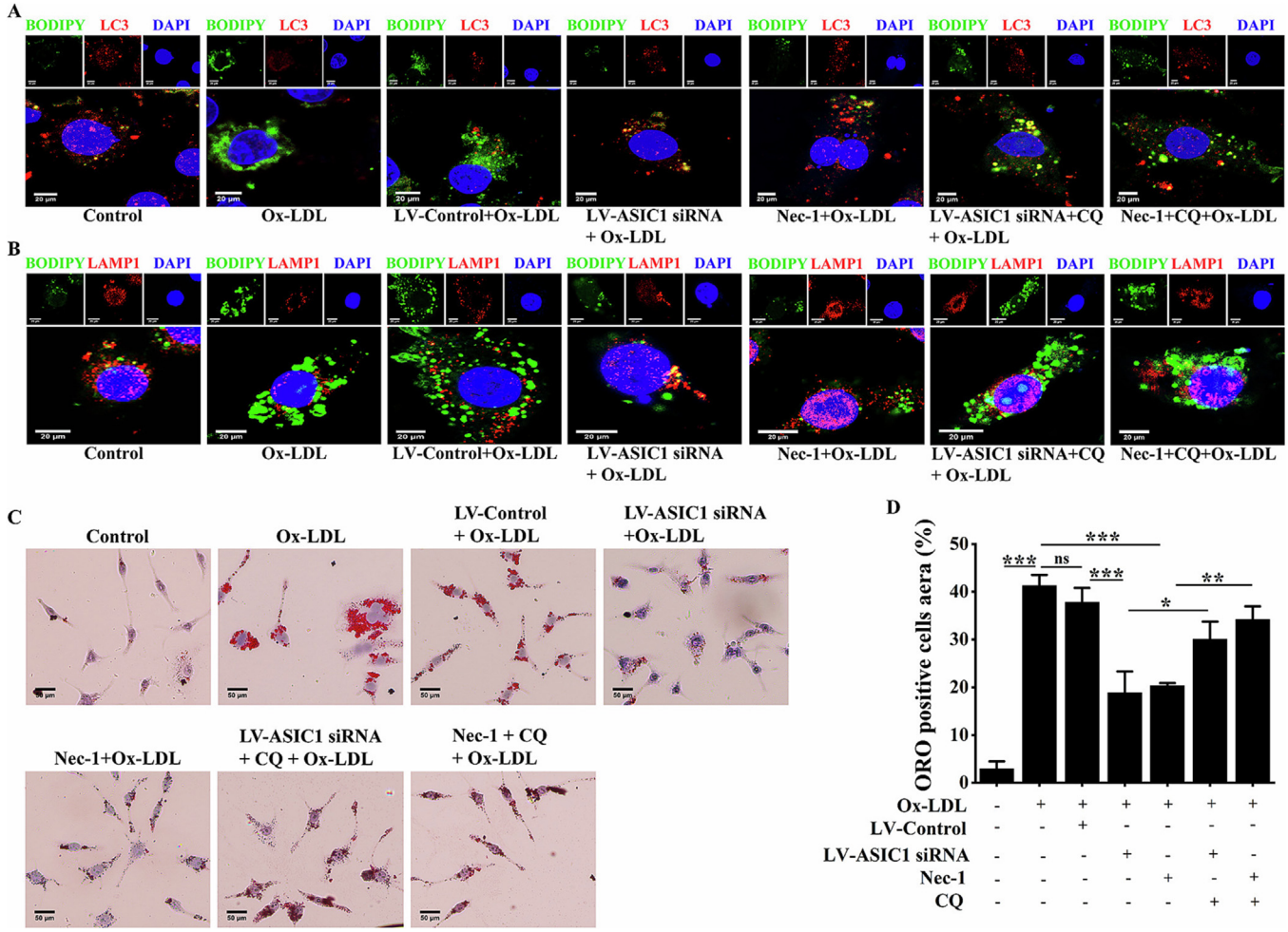

Fig. 4. *Influence of ASIC1/RIP1 on lipophagy and lipid accumulation in RAW 264.7 macrophages.* Macrophages were treated with LV-Control or LV-ASIC1 siRNA for 48 h. Subsequently, the cells were divided into 7 groups: Control, ox-LDL, LV-Control + ox-LDL, LV-ASIC1 siRNA + ox-LDL, Nec-1 + ox-LDL, LV-ASIC1 siRNA + CQ and Nec-1 + CQ. (A, B) Representative confocal image of the colocalization of BODIPY with LC3II (A) and LAMP1. (B) RAW 264.7 macrophages. Scale bar, 2 μm. (C) Representative ORO staining images of RAW264.7 macrophages. (D) Quantification of ORO. Scale bar, 50 μm. All data are presented as the mean ± SEM from 3 to 5 independent experiments. $^{*}P < 0.05$, $^{**}P < 0.01$, $^{***}P < 0.001$.

atherosclerosis but also position ASIC1 as a promising therapeutic target for atherosclerotic diseases.

The wild-type mouse exhibits resistance to atherogenesis, whereas the ApoE$^{-/-}$ mouse spontaneously develops atherosclerosis with morphological features and distribution similar to that seen in humans. Consequently, in the current study, we utilized ApoE$^{-/-}$ mouse atherosclerosis models. Our research underscores the pivotal role of ASIC1 in the development of atherosclerosis. Previous studies have provided evidence that ASIC1 is abundantly expressed in RAW 264.7 macrophages, where it acts as an extracellular proton sensor. This function triggers the activation of downstream signaling pathways, subsequently leading to a cascade of pathophysiological changes [25]. Our prior research has already established that extracellular acidity plays a role in promoting the formation of macrophage-derived foam cells through the activation of ASIC1. This suggests that this channel protein is indeed implicated in the pathological processes underlying atherosclerosis [9]. Despite our previous findings, which strongly suggested a role for ASIC1 in promoting atherogenesis through in vitro studies, in vivo evidence supporting this hypothesis was lacking. In this study, we employed scRNA-seq database analyses, which revealed the presence of ASIC1 mRNA in multiple cell clusters within human atherosclerotic lesions. However, our immunofluorescence staining assays provided a crucial clarification - the expression of ASIC1 protein was predominantly observed in macrophages located within atherosclerotic lesions, a pattern consistent in both ApoE$^{-/-}$ mice and human patients. Notably, ASIC1 deficiency had a significant impact, resulting in decreased lipid accumulation in RAW264.7 macrophages and reduced atherosclerotic lesions in ApoE$^{-/-}$ mice. These compelling results strongly suggest a pro-atherosclerotic role for ASIC1.

Crucially, this study provides clarification on how ASIC1 contributes to the impairment of lipophagy in macrophages when faced with hyperlipidemia or ox-LDL. Macrophage-derived foam cells are key components of atherosclerotic plaques, and their formation represents a pivotal initial step in the development of atherosclerosis [26]. Growing evidence supports the notion that lipophagy plays an anti-atherosclerotic role by promoting the hydrolysis of cholesterol esters and subsequent efflux of free cholesterol [27,28]. Recent studies have also demonstrated that defective lipophagy exacerbates intracellular lipid accumulation and the progression of atherosclerotic lesions [29]. Furthermore, previous reports have confirmed that ASIC1-mediated abnormal autophagy contributes to senescence and apoptosis in rat articular chondrocytes [30,31]. In our scRNA-seq analysis, we indeed observed impairment in the autophagy–lysosome-associated pathway in atherosclerotic lesions. Moreover, we identified increased ASIC1 expression in macrophages situated within atherosclerotic

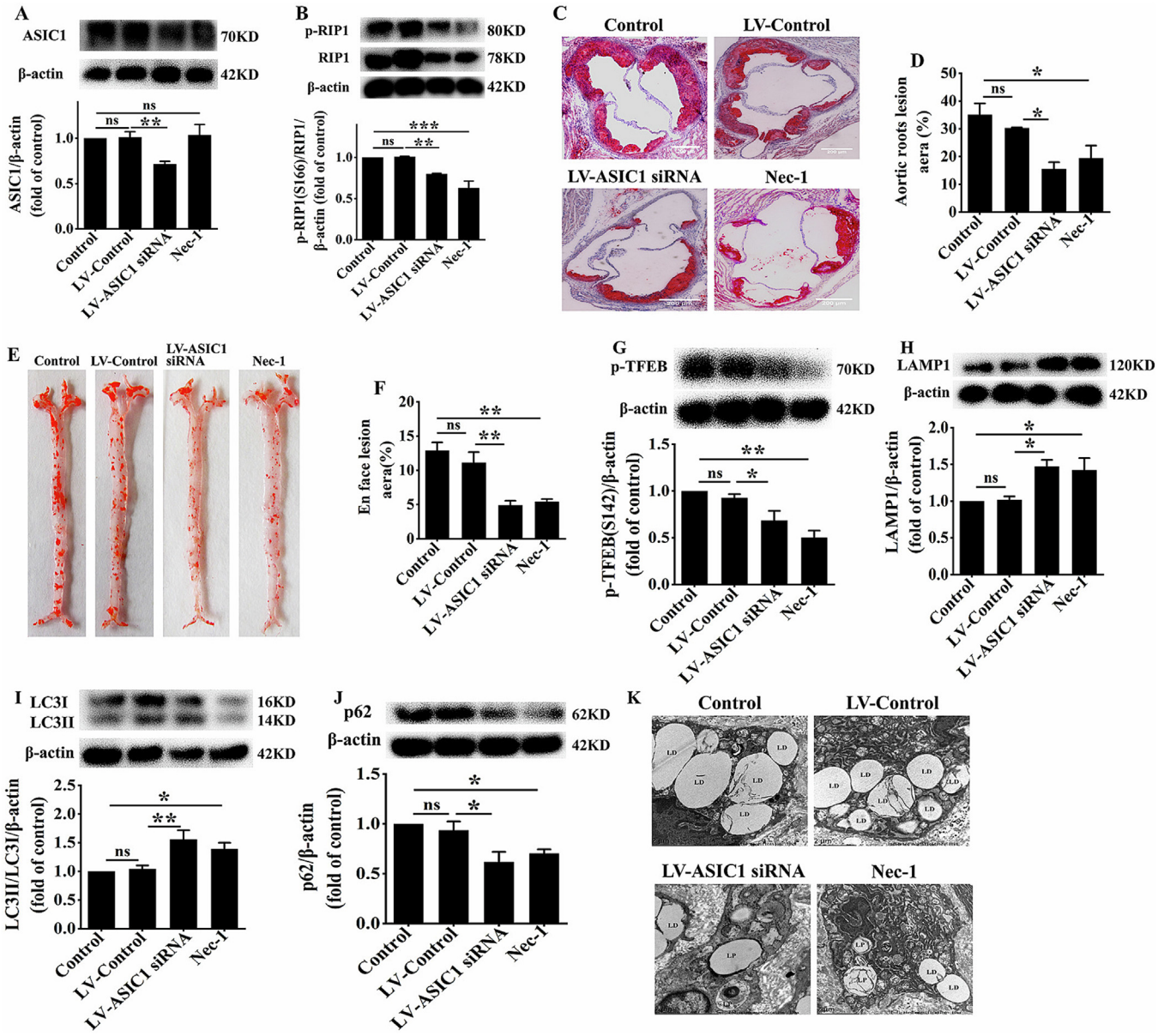

Fig. 5. *Effect of ASIC1/RIP1 inhibition on lipophagy in atherosclerotic lesions of ApoE$^{-/-}$ mice.* ApoE$^{-/-}$ mice were fed a high-feed diet for 12 weeks to induce atherosclerotic lesions. During this time, Nec-1 was administered daily, and lentivirus infection was conducted in the second week. (A, B) Western blotting analyses were carried out to evaluate ASIC1 protein and p-RIP levels in extracts from the whole aortas of ApoE$^{-/-}$ mice. (C) Representative ORO staining images of aortic roots in the indicated groups. Scale, 200 μm. (D) Quantitative analysis of the ORO staining area. (E) Representative ORO staining images of whole aortas. (F) Quantitative analysis of ORO staining areas. (G–J) p-TFEB, LAMP1, LC3I, LC3II and p62 levels in aortas ApoE$^{-/-}$ mice were detected by western blot analysis. (K) Changes in lipophagy in the aortic roots of mice were observed by transmission electron microscopy. LD: lipid droplet, LP: lipophagosome. Scale bar, 2 μm. All data are presented as the mean ± SEM. $^{*}P < 0.05$, $^{**}P < 0.01$, $^{***}P < 0.001$.

plaques, coinciding with disrupted lipophagy. Therefore, we further explored the role of ASIC1 in defective lipophagy within macrophages. Our results clearly demonstrated that ASIC1 knockdown substantially restored lipophagy in macrophages exposed to ox-LDL and in aortic cells within atherosclerotic plaques. This suggests that the activation of ASIC1 in macrophages inhibits autophagy, which contrasts with other reports that ASIC1 increased autophagy activity in acid-induced rat articular chondrocytes or gastric cancer cells [31,32]. This discrepancy may arise from the fact that ASIC1 activation in different cell types has varying effects on the autophagy pathway. Furthermore, we observed that the role of ASIC1 deficiency in promoting macrophage lipophagy was counteracted by the autophagy–lysosome inhibitor CQ. Alongside the observation of decreased lipid accumulation in macrophages and atherosclerotic lesions in ApoE$^{-/-}$ mice induced by ASIC1 silencing, these results underscore that ASIC1 accelerates atherogenesis by disrupting macrophage lipophagy.

We then explored the mechanism by which ASIC1 promoted lipophagy deficiency in macrophages. Our findings demonstrate that the RIP1/TFEB signaling pathway is implicated in ASIC1-mediated macrophage lipophagy impairment. While RIP1 is well known as a critical mediator in necrotic cell death, recent studies have indicated that its activation inhibits autophagy by impeding TFEB nuclear localization [14]. Previous studies have shown that the kinase activity of RIP1 is determined by its autophosphorylation sites, such as Ser161 and Ser166 [33,34]. Among these phosphorylated RIP1, RIP1-Ser166 levels are positively correlated with RIP1 activity [35]. Interestingly, Wang YZ et al showed that in the ischemic brain, ASIC1 interacted with RIP1 to cause autophosphorylation of RIP1, which further triggered downstream molecu-

lar events [15]. Thus, in the present study, we investigated whether a similar mechanism occurred in macrophages exposed to ox-LDL. The results indicated that ox-LDL promoted ASIC1/RIP1 association and increased RIP1-Ser166 levels in RAW264.7 macrophages. However, all of these events were abolished by PcTx-1, a specific inhibitor of ASIC1 activation. These findings imply that RIP1-Ser166 can result from ASIC1/RIP1 association in macrophages exposed to ox-LDL, which is consistent with the results of Wang et al. [15].

Furthermore, our investigation revealed a significant increase in the levels of p-TFEB Ser-142 in both RAW 264.7 macrophages and aortas from ApoE$^{-/-}$ mice. This was accompanied by a subsequent decrease in the protein expression of LC3 and LAMP1. Importantly, these effects were all effectively reversed by ASIC1 silencing and RIP1 inhibition. These findings illuminate that proatherogenic factors such as ox-LDL and hyperlipidemia hinder macrophage autophagy through the activation of ASIC1/RIP1, leading to enhanced TFEB phosphorylation. Additionally, our study identified that when the ASIC1/RIP1 pathway was inhibited, the restoration of autophagic flux coincided with a significant increase in the colocalization of lipid droplets (LDs) with autophagosomes and lysosomes. Simultaneously, there was a marked reduction in lipid accumulation within the macrophages. In summary, these results strongly support the notion that macrophage ASIC1 disrupts lipophagy through the activation of RIP1, leading to an increase in phosphorylation at serine 142 of TFEB. A limitation of this study is that we explored the proatherogenic effect of ASIC1 in ApoE$^{-/-}$ mice using only siRNA and not using an ASIC1 knockout strategy to validate our findings.

In conclusion, our study explores the critical role and underlying mechanism of ASIC1 in atherosclerosis. The findings clarify that ASIC1 activation exacerbates macrophage lipid accumulation and atherogenesis by disrupting lipophagy. In proatherosclerotic conditions, ASIC1 interacts with RIP1 to cause the phosphorylation of TFEB, decreasing the expression of the autophagy–lysosome-associated proteins LC3 and Lamp1 and thereby impeding macrophage lipophagy. Our results reveal a novel mechanism by which ASIC1 contributes to atherosclerosis by inhibiting macrophage lipophagy. Targeting macrophage ASIC1 may be a novel therapeutic strategy for atherosclerosis. However, most data presented herein were mainly derived from cell or animal models. A key impediment to the appreciation of targeting ASICl as a potential disease treatment is the lack of clinical evidence. Furthermore, the small molecule blockers of ASICs that are currently available exhibit low selectivity for individual ASIC1 subunits. With a better understanding of the structure and function of this channel, the development of ASIC1-specific and potent blockers to treat and prevent atherosclerosis will hopefully enter clinical studies in the near future.

CRediT authorship contribution statement

Yuan-Mei Wang: Investigation, Formal analysis, Investigation, Visualization, Writing – original draft. **Huang Tang:** Conceptualization, Writing – original draft. **Ya-Jie Tang:** Conceptualization, Writing – review & editing. **Juan Liu:** Investigation, Visualization, Validation. **Yu-Fang Yin:** Writing – review & editing. **Ya-Ling Tang:** Resources. **Yao-Guang Feng:** Resources. **Hong-Feng Gu:** Investigation, Project administration, Writing – original draft, Supervision, Validation, Funding acquisition.

Declaration of competing interest

The authors declare the following financial interests/personal relationships which may be considered as potential competing interests: No conflict of financial or proprietary interest exits in the submission of this manuscript, and this manuscript has not been submitted elsewhere for publication, in whole or in part. All the authors listed have approved the publication of this manuscript.

Acknowledgments

This work was supported by grants from the National Natural Science Foundation of China (grant no. 81500349), the Key Research and Development Program of Hunan Province (2019SK2021), the Natural Science Foundation of Hunan Province, China (grant no. 2022JJ30509), the Key Program of Educational Commission of Hunan Province, China (grant no. 21A0273), and the Health and Family Planning Commission of Hunan Province, China (grant no. B2017048).

Appendix A. Supplementary material

Supplementary data to this article can be found online at https://doi.org/10.1016/j.jare.2023.11.004.

References

[1] Zhang RJ, Yin YF, Xie XJ, Gu HF. Acid-sensing ion channels: linking extracellular acidification with atherosclerosis. Clin Chim Acta 2020;502:183–90. doi: https://doi.org/10.1016/j.cca.2019.12.027.
[2] Lee-Rueckert M, Lappalainen J, Leinonen H, Plihtari R, Nordstrom T, Akerman K, et al. Acidic extracellular pH promotes accumulation of free cholesterol in human monocyte-derived macrophages via inhibition of ACAT1 activity. Atherosclerosis 2020;312:1–7. doi: https://doi.org/10.1016/j.atherosclerosis.2020.08.011.
[3] Liu CL, Zhang X, Liu J, Wang Y, Sukhova GK, Wojtkiewicz GR, et al. Na(+)-H(+) exchanger 1 determines atherosclerotic lesion acidification and promotes atherogenesis. Nat Commun 2019;10:3978. doi: https://doi.org/10.1038/s41467-019-11983-3.
[4] Lynagh T, Flood E, Boiteux C, Sheikh ZP, Allen TW, Pless SA. Determinants of ion selectivity in ASIC1a- and ASIC2a-containing acid-sensing ion channels. J Gen Physiol 2020;152. doi: https://doi.org/10.1085/jgp.201812297.
[5] Jernigan NL. Smooth muscle acid-sensing ion channel 1: pathophysiological implication in hypoxic pulmonary hypertension. Exp Physiol 2015;100:111–20. doi: https://doi.org/10.1113/expphysiol.2014.081612.
[6] Alvarez de la Rosa D, Krueger SR, Kolar A, Shao D, Fitzsimonds RM, Canessa CM. Distribution, subcellular localization and ontogeny of ASIC1 in the mammalian central nervous system. J Physiol 2003;546:77–87. doi: https://doi.org/10.1113/jphysiol.2002.030692.
[7] Lee C.S., O'Sullivan W.J. The interaction of phosphorothioate analogs of ATP with phosphomevalonate kinase. Kinetic and 31P NMR studies. J Biol Chem 1985;260:13909–13915. IF: 4.8 Q2.
[8] Ding J, Chen Y, Zhao YJ, Chen F, Dong L, Zhang HL, et al. Acid-sensitive ion channel 1a mediates osteoarthritis chondrocyte senescence by promoting Lamin B1 degradation. Biochem Pharmacol 2022;202:115107. doi: https://doi.org/10.1016/j.bcp.2022.115107.
[9] Wang YM, Tan MY, Zhang RJ, Qiu MY, Fu YS, Xie XJ, et al. Acid-sensing ion channel 1/calpain1 activation impedes macrophage ATP-binding cassette protein A1-mediated cholesterol efflux induced by extracellular acidification. Front Physiol 2021;12:777386. doi: https://doi.org/10.3389/fphys.2021.777386.
[10] Zhang CJ, Zhu N, Long J, Wu HT, Wang YX, Liu BY, et al. Celastrol induces lipophagy via the LXRalpha/ABCA1 pathway in clear cell renal cell carcinoma. Acta Pharmacol Sin 2021;42:1472–85. doi: https://doi.org/10.1038/s41401-020-00572-6.
[11] Pi S, Mao L, Chen J, Shi H, Liu Y, Guo X, et al. The P2RY12 receptor promotes VSMC-derived foam cell formation by inhibiting autophagy in advanced atherosclerosis. Autophagy 2021;17:980–1000. doi: https://doi.org/10.1080/15548627.2020.1741202.
[12] Medina DL, Di Paola S, Peluso I, Armani A, De Stefani D, Venditti R, et al. Lysosomal calcium signaling regulates autophagy through calcineurin and TFEB. Nat Cell Biol 2015;17:288–99. doi: https://doi.org/10.1038/ncb3114.
[13] Settembre C, Di Malta C, Polito VA, Garcia Arencibia M, Vetrini F, Erdin S, et al. TFEB links autophagy to lysosomal biogenesis. Science 2011;332:1429–33. doi: https://doi.org/10.1126/science.1204592.
[14] Abe K, Yano T, Tanno M, Miki T, Kuno A, Sato T, et al. mTORC1 inhibition attenuates necroptosis through RIP1 inhibition-mediated TFEB activation. Biochim Biophys Acta Mol Basis Dis 2019;1865:165552. doi: https://doi.org/10.1016/j.bbadis.2019.165552.
[15] Wang YZ, Wang JJ, Huang Y, Liu F, Zeng WZ, Li Y, et al. Tissue acidosis induces neuronal necroptosis via ASIC1a channel independent of its ionic conduction. Elife 2015;4. doi: https://doi.org/10.7554/eLife.05682.
[16] Zhou R, Wu X, Wang Z, Ge J, F.. Chen Interleukin-6 enhances acid-induced apoptosis by upregulating acid-sensing ion channel 1a expression and

function in rat articular chondrocytes. Int Immunopharmacol 2015;29:748–60. doi: https://doi.org/10.1016/j.intimp.2015.08.044.
[17] Butler A, Hoffman P, Smibert P, Papalexi E, R.. Satija Integrating single-cell transcriptomic data across different conditions, technologies, and species. Nat Biotechnol 2018;36:411–20. doi: https://doi.org/10.1038/nbt.4096.
[18] Wu T, Hu E, Xu S, Chen M, Guo P, Dai Z, et al. clusterProfiler 4.0: A universal enrichment tool for interpreting omics data. Innovation (Camb) 2021;2:100141. doi: https://doi.org/10.1016/j.xinn.2021.100141.
[19] Xue Y, Luo M, Hu X, Li X, Shen J, Zhu W, et al. Macrophages regulate vascular smooth muscle cell function during atherosclerosis progression through IL-1beta/STAT3 signaling. Commun Biol 2022;5:1316. doi: https://doi.org/10.1038/s42003-022-04255-2.
[20] Zafar A, Pong Ng H, Diamond-Zaluski R, Kim GD, Ricky Chan E, Dunwoodie SL, et al. CITED2 inhibits STAT1-IRF1 signaling and atherogenesis. FASEB J 2021;35:e21833.
[21] Gao WF, Xu YY, Ge JF, Chen FH. Inhibition of acid-sensing ion channel 1a attenuates acid-induced activation of autophagy via a calcium signaling pathway in articular chondrocytes. Int J Mol Med 2019;43:1778–88. doi: https://doi.org/10.3892/ijmm.2019.4085.
[22] Yonekawa T, Gamez G, Kim J, Tan AC, Thorburn J, Gump J, et al. RIP1 negatively regulates basal autophagic flux through TFEB to control sensitivity to apoptosis. EMBO Rep 2015;16:700–8. doi: https://doi.org/10.15252/embr.201439496.
[23] Pan B, Li J, Parajuli N, Tian Z, Wu P, Lewno MT, et al. The calcineurin-TFEB-p62 pathway mediates the activation of cardiac macroautophagy by proteasomal malfunction. Circ Res 2020;127:502–18. doi: https://doi.org/10.1161/CIRCRESAHA.119.316007.
[24] Wang K, Zhang T, Lei Y, Li X, Jiang J, Lan J, et al. Identification of ANXA2 (annexin A2) as a specific bleomycin target to induce pulmonary fibrosis by impeding TFEB-mediated autophagic flux. Autophagy 2018;14:269–82. doi: https://doi.org/10.1080/15548627.2017.1409405.
[25] Ni L, Fang P, Hu ZL, Zhou HY, Chen JG, Wang F, et al. Identification and function of acid-sensing ion channels in RAW 264.7 macrophage cells. Curr Med Sci 2018;38:436–42. doi: https://doi.org/10.1007/s11596-018-1897-y.
[26] Robichaud S, Rasheed A, Pietrangelo A, Doyoung Kim A, Boucher DM, Emerton C, et al. Autophagy is differentially regulated in leukocyte and nonleukocyte foam cells during atherosclerosis. Circ Res 2022;130:831–47. doi: https://doi.org/10.1161/CIRCRESAHA.121.320047.
[27] Shan R, Liu N, Yan Y, B.. Liu Apoptosis, autophagy and atherosclerosis: Relationships and the role of Hsp27. Pharmacol Res 2021;166:105169. doi: https://doi.org/10.1016/j.phrs.2020.105169.
[28] Xiaolong L, Dongmin G, Liu M, Zuo W, Huijun H, Qiufen T, et al. FGF21 induces autophagy-mediated cholesterol efflux to inhibit atherogenesis via RACK1 upregulation. J Cell Mol Med 2020;24:4992–5006. doi: https://doi.org/10.1111/jcmm.15118.
[29] Zhao T, Wu K, Hogstrand C, Xu YH, Chen GH, Wei CC, et al. Lipophagy mediated carbohydrate-induced changes of lipid metabolism via oxidative stress, endoplasmic reticulum (ER) stress and ChREBP/PPARgamma pathways. Cell Mol Life Sci 2020;77:1987–2003. doi: https://doi.org/10.1007/s00018-019-03263-6.
[30] Xie YY, Li Y, Zhou RP, Dai BB, Qian YJ, Wu XS, et al. Effects of autophagy on acid-sensing ion channel 1a-mediated apoptosis in rat articular chondrocytes. Mol Cell Biochem 2018;443:181–91. doi: https://doi.org/10.1007/s11010-017-3223-6.
[31] Song SJ, Tao JJ, Li SF, Qian XW, Niu RW, Wang C, et al. 17beta-estradiol attenuates rat articular chondrocyte injury by targeting ASIC1a-mediated apoptosis. Mol Cell Endocrinol 2020;505:110742. doi: https://doi.org/10.1016/j.mce.2020.110742.
[32] Zhang Q, Wu S, Zhu J, Chai D, Gan H. Downregulation of ASIC1 suppressed gastric cancer by inhibiting autophagy. Gene 2017;608:79–85. doi: https://doi.org/10.1016/j.gene.2017.01.014.
[33] Zhang Y, Su SS, Zhao S, Yang Z, Zhong CQ, Chen X, et al. RIP1 autophosphorylation is promoted by mitochondrial ROS and is essential for RIP3 recruitment into necrosome. Nat Commun 2017;8:14329. doi: https://doi.org/10.1038/ncomms14329.
[34] Zhou Y, Liao J, Mei Z, Liu X, Ge J. Insight into crosstalk between ferroptosis and necroptosis: novel therapeutics in ischemic stroke. Oxid Med Cell Longev 2021;2021:9991001. doi: https://doi.org/10.1155/2021/9991001.
[35] Laurien L, Nagata M, Schunke H, Delanghe T, Wiederstein JL, Kumari S, et al. Autophosphorylation at serine 166 regulates RIP kinase 1-mediated cell death and inflammation. Nat Commun 2020;11:1747. doi: https://doi.org/10.1038/s41467-020-15466-8.